

Title

Subtitle

by

Mikkel Metzsch Jensen

THESIS

for the degree of

MASTER OF SCIENCE



Faculty of Mathematics and Natural Sciences
University of Oslo

Spring 2023

Title

Subtitle

Mikkel Metzsch Jensen

© 2023 Mikkel Metzsch Jensen

Title

<http://www.duo.uio.no/>

Printed: Reprosentralen, University of Oslo

Abstract

Abstract.

Acknowledgments

Acknowledgments.

Contents

List of symbols?	vii
I Background Theory	1
II Simulations	3
1 Pilot study	5
1.1 Friction simulation parameters	5
1.1.1 Pressure reference for normal load domain	7
1.2 Single friction simulation analysis	8
1.2.1 Force oscillations	8
1.2.2 Decompositions	9
1.2.3 Center of mass path	10
1.3 Defining metrics for dynamic and static friction	11
1.3.1 Dynamic friction	11
1.3.2 Static friction	12
1.4 Out of plane buckling	13
1.5 Investigating selected parameters	15
1.6 Normal force and stretch dependencies	17
1.6.1 Contact area	18
1.6.2 Stretch	18
1.6.3 Normal force	20
1.7 Computational cost	21
2 Dataset study	23
2.1 Generating data	23
2.2 Data analysis	23
2.3 Properties of interest / Stretch profiles	25
2.4 Machine learning	28
2.5 Accelerated Search	28
2.5.1 Markov-Chain Accelerated Genetic Algorithms	28
2.5.1.1 Talk about traditional method also?	28
2.5.1.2 Implementing for 1D chromosome (following article closely)	28
Summary	31
2.6 Summary and conclusion	31
2.7 Outlook / Perspective	31
Appendices	33
Appendix A	35

List of symbols?

Maybe add list of symbols and where they are used like Trømborg.

Part I

Background Theory

Part II

Simulations

Chapter 1

Pilot study

1.1 Friction simulation parameters

The friction simulation is governed by a set of parameters where some is kept constant while other is varied to gain insight in the frictional properties. These parameters can be categorised into three main categories of different purpose as described in table 1.1.

Table 1.1: Parameters of the numerical procedure for measuring friction.

Category	Parameter name: description	Category purpose
Physical	<ul style="list-style-type: none"> - T: Temperature for the Langevin thermostat. - v_{slide} : Sliding speed for the sheet translation. - K: Spring constant for the spring force between the virtual atom and the pull blocks responsible for translating the sheet along the substrate. An infinite spring constant is achieved by moving the pull blocks as a rigid body (Lammps: fix move). - Scan angle: The direction for which we translate the sheet. 	Parameters expected to have a physical effect on the friction properties, which is kept fixed and thus not included in the machine learning input set.
Measurement	<ul style="list-style-type: none"> - dt: Integration timestep. - t_R: Relaxation time before stretching. - Pauses between stretch and adding normal force and between dragging the sheet. - Stretch Speed: How fast to stretch the sheet. - Slide distance: How far to translate the sheet. - Sheet size: Spatial size of the 2D sheet. - Pull block size: spatial size of the pull blocks. 	Parameters influencing the simulation dynamics and being representative of the experimental procedure that we are mimicking. These parameters are chosen with the aim of getting stable parameters under small perturbations of the given parameter.
ML input	<ul style="list-style-type: none"> - Sheet configuration: A binary matrix containing information of which atoms are removed (0) and which are still present (1) in the graphene sheet. - Stretch amount: The relative sheet stretch in percentage. - F_N: Applied normal force to the pull blocks. 	The remaining parameters serve as input variables for optimization process and is thus given as input variables for the machine learning (ML).

Due to the great number of parameters, and corresponding range of reasonable numerical values they can take, it is ... to parameter search including all of these. Thus, we will to a great extent rely on a reverse engineering in order to establish a set of parameters for the *physical* and *measurement* categories along with numerical ranges for the *ML input* category which gives stable and promising results. By doing so we effectively narrow down the parameter regime for which the investigated frictional properties belong. We aim to choose the parameters in order to accommodate a balance between generalizable and stable result which is simultaneously a suitable candidate as a proof of concept for the control of friction properties using kirigami inspired cuts.

In the following we present the results of the friction simulations in parallel to the procedure of investigating the choice of different parameters.

In the following subsections (X to Y) we are going to present the friction simulation results in parallel to the presentation of the reasoning behind the parameter choices. For this we will refer to the default parameter choice showcased in table 1.2 which is representative of the final parameter choices.

Table 1.2: Final parameters for the friction simulations Probably not the neatest format for this...

Physical	Measurements	ML input
$T = 300 \text{ K}$ $v_{\text{slide}} = 20 \text{ m/s}$ $K = \text{inf}$ (LAMMPS: <i>fix move</i>) Scan angle : $(x, y) = (0, 1)$	$dt = 1 \text{ fs}$ $t_R = 15 \text{ ps}$ Pauses = 5 ps Stretch speed = 0.01 ps^{-1} Slide distance = 400 \AA Sheet size = $130.029 \times 163.219 \text{ \AA}$ Pull block size = $2 \times 130.029 \times 15.183 \text{ \AA}$	Sheet configuration = Contiguous Stretch amount = Below rupture $F_N = [0.1, 10] \text{ nN}$

Say something about how these parameters are chosen. Reference to articles for which these were mirrored from.

1.1.1 Pressure reference for normal load domain

Find place to put this.

In order to relate the magnitude of the normal force in our friction measurement we will use the pressure as a reference. We will use the pressure underneath a stiletto shoe as a worst case for human pressure execution underneath the shoe. From (source 1) it is reported that the diameter of a stiletto heeled shoe can be less than 1 cm. Hence a 80 kg man¹ standing on one stiletto heel (with all the weight on the heel) will result in a pressure

$$P = \frac{F}{A} = \frac{mg}{r^2\pi} = \frac{80 \text{ kg} \cdot 9.8 \frac{\text{m}}{\text{s}^2}}{(\frac{1 \times 10^{-2} \text{ m}}{2})^2\pi} = 9.98 \text{ MPa}$$

While this is in itself a spectacular realization that is often used in introductory physics courses (source 2) to demonstrate the rather extreme pressure under a stiletto heel (greater than the foot of an elephant) (how many Atmos?) this serves as a reasonable upperbound for human executed pressure. With a full sheet area of $\sim 21 \times 10^3 \text{ \AA}^2$ we can achieve a similar pressure of $\sim 10 \text{ MPa}$ with a normal force of

$$F_N = 10 \text{ MPa} \cdot 21 \times 10^{-17} \text{ m}^2 = 2.10 \text{ nN}$$

Of course this pressure might be insufficient for various industrial purposes, but with no specific procedure in mind this serves as a decent reference point. Notice that if we consider a human foot with area 113 cm^2 the pressure drops to a mere 70 kPa corresponding to $\sim 0.01 \text{ nN}$.

¹Yes, a man can certainly wear stiletto heels.

1.2 Single friction simulation analysis

We begin by assessing the raw data for a single friction simulation run with the default parameters shown in table 1.2 for a non-cut sheet, no stretch and an applied normal force of 1 nN.

1.2.1 Force oscillations

We first assess the raw data for the friction force F_{\parallel} parallel to the drag direction as seen in figure 1.1. The sample rate is $10 \text{ ps}^{-1} = 100 \text{ timesteps}^{-1}$ for which each sample is the mean value of the 100 timesteps preceding the given sample interval. We observe immediately that the data carries oscillations on different time scales. By applying a savgol filter to the data with a polyorder of 5 and window length of 150 timesteps, corresponding to a sliding distance of 3 Å or a time window of 15 ps, we can qualitatively point out at least two different frequencies of oscillation. On figure 1.1a we see roughly three waves on the savgol filter corresponding to a relative high frequency, while on 1.1b the same savgol filter reveals a lower frequency on top of the first, creating the visual pattern of a wavepacket.

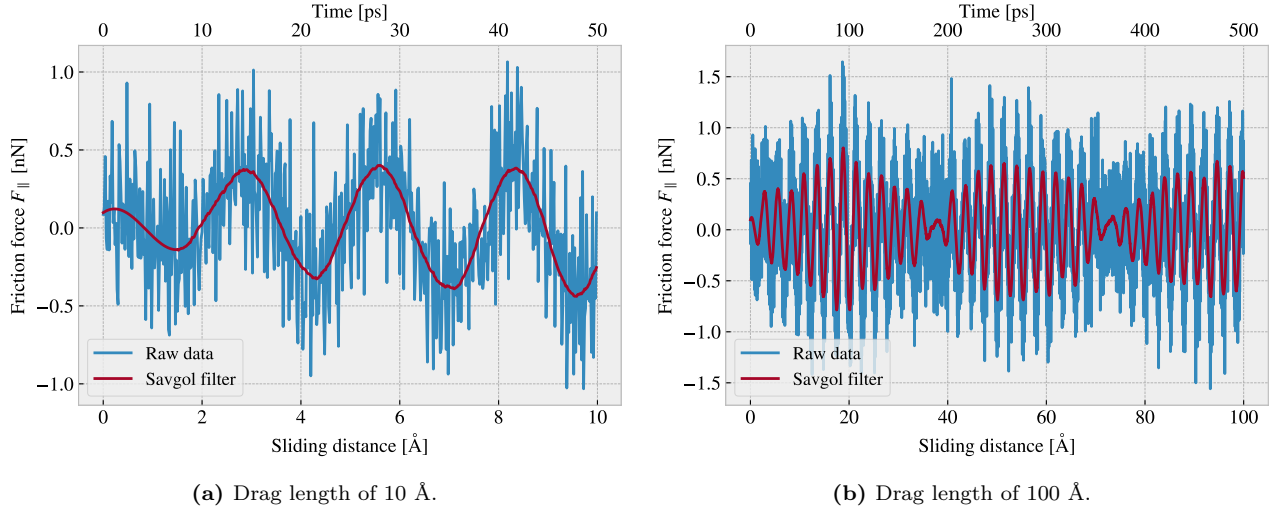


Figure 1.1: Friction force F_{\parallel} with respect to the drag direction between (full) sheet and substrate versus sliding distance. The sliding distance is measured by the constant movement of the virtual atom and not the COM of the sheet. However, we expect these measures to be fairly identical due to the fact that the pull blocks are rigidly coupled to the virtual atom. The red line represents a savgol filter with window polyorder 5 and window length of 150 timesteps (corresponding to a sliding distance of 3 Å or a time window of 15 ps).

By performing a Fourier Transform (FT) on the data we can quantify the leading frequencies as seen in figure 1.2a. By plotting the two most dominant frequencies $f_1 = 0.0074 \text{ ps}^{-1}$ and $f_2 = 0.0079 \text{ ps}^{-1}$ as $\sin(2\pi f_1) + \sin(2\pi f_2)$ we find a qualitatively convincing fit to the observed wavepacket shape as seen in figure 1.2b. By using the trigonometric identity

$$\begin{aligned}\sin(\alpha + \beta) &= \sin(\alpha)\cos(\beta) + \cos(\alpha)\sin(\beta), \\ \sin(\alpha - \beta) &= \sin(\alpha)\cos(\beta) - \cos(\alpha)\sin(\beta),\end{aligned}$$

and decomposing $f_1 = a - b$, $f_2 = a + b$ we can rewrite the sine sum as the sinusoidal product

$$\begin{aligned}\sin(2\pi f_1) \sin(2\pi f_2) &= \sin(2\pi(a - b)) \sin(2\pi(a + b)) \\ &= \sin(a)\cos(b) + \cancel{\cos(2\pi a)\sin(2\pi b)} + \sin(2\pi a)\cos(2\pi b) - \cancel{\cos(2\pi a)\sin(2\pi b)} \\ &= 2\sin(2\pi a)\cos(2\pi b),\end{aligned}$$

with

$$\begin{aligned}a &= \frac{f_1 + f_2}{2} = 0.0763 \pm 0.0005 \text{ ps}^{-1}, & b &= \frac{f_2 - f_1}{2} = 0.0028 \pm 0.0005 \text{ ps}^{-1}, \\ &= 0.381 \pm 0.003 \text{ Å}^{-1}, & &= 0.014 \pm 0.003 \text{ Å}^{-1},\end{aligned}$$

where the latter frequency is denoted with respect to the sliding distance. This makes us recognize the high oscillation frequency as a and the low frequency as b . The faster one has a period of $T_a = 2.62 \pm 0.02 \text{ \AA}^2$. This corresponds well with the magnitude of the lattice spacing and especially that of graphene at 2.46 \AA as expected theoretically (make reference to theory section?). We also take note of the longest period $T_b = 71 \pm 15 \text{ \AA}^{-1}$ which will be relevant for the evaluation of measurement uncertainty in section 1.3.

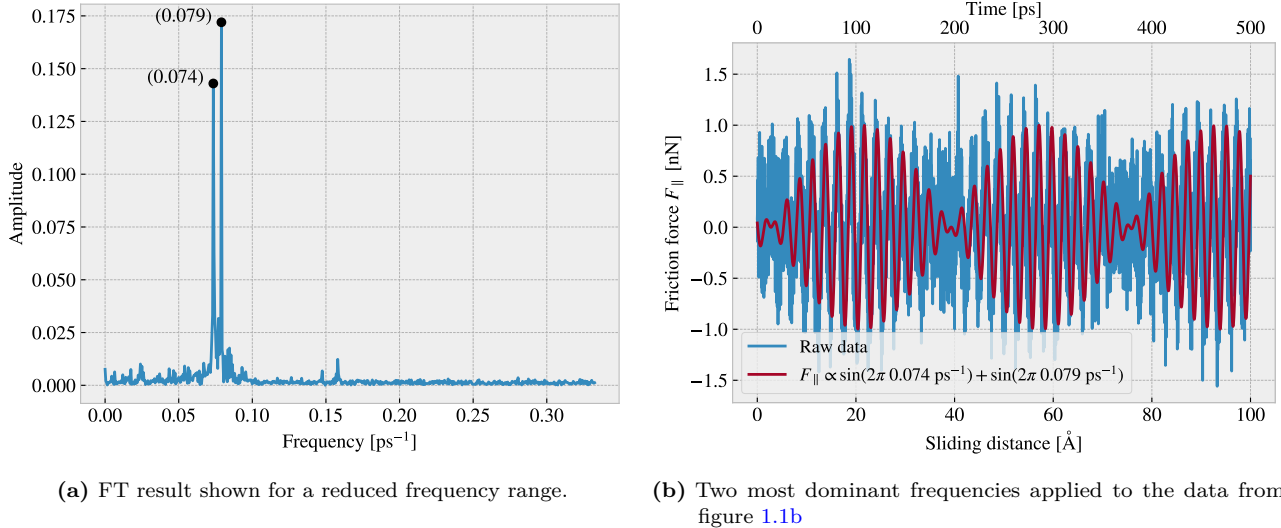


Figure 1.2: Fourier transform (FT) analysis of the full friction force data (all 400 \AA sliding distance) shown in figure 1.1. (a) shows the two most dominant frequency peaks. Note that no significant peaks were found in a higher frequency than included here. (b) shows a comparison between the raw data and the wavefunction corresponding to the two peaks in figure (a).

1.2.2 Decompositions

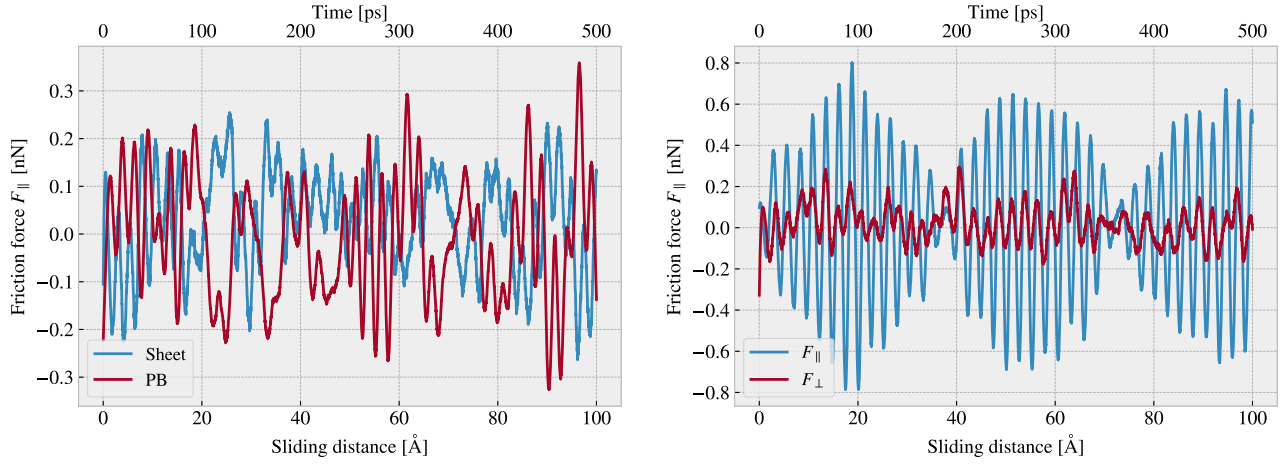
In the previous analysis we have looked only at the friction force for the full sheet, including the pull blocks which is locked off during sliding, and with respect to the drag direction. This represents our choice measurement which we will address in the following.

Due to the fact that we are only applying cuts to the inner sheet (excluding the pull blocks), it might seem more natural to only consider the friction on that part. If the desired frictional properties can be achieved by altering the inner sheet one can argue that any opposing effects from the pull blocks can be mitigated by scaling the relative size between the inner sheet and the pull blocks. However, when looking at the time series of the friction force decomposed with respect to the inner sheet and pull block region (see figure 1.3a), we observe the friction force arising from those parts are seemingly antisymmetric. That is, the distribution of the frictional pull from the substrate on the sheet is oscillating between the inner sheet and the pull block. Keeping in mind that normal force is only applied to the pull blocks we might take this as an integrated feature of the system which does not necessarily disappear when changing the spatial ratio between inner sheet and pull block. Any interesting friction properties might depend on this internal distribution of forces. Hence, we hedge our bets and use the full sheet friction force as a holistic approach to this measurement problem.

Similar we might question the decision of only considering the frictional force projected onto the sliding direction as we are neglecting the “side shift” induced during the slide phase. In figure 1.3b we see the decomposition into force components parallel F_{\parallel} and perpendicular F_{\perp} to the slide direction respectively. We see that the most dominant trend is projected into the parallel component. If we want to include the perpendicular component as well we would have to evaluate the friction as the length of the force vector for which we would lose the sign of the force direction. Hence, we would only get a positive contribution which would not be able to capture the change between resisting and assisting the sliding during stick-slip motion. One option to accommodate this is by using the vector length but keeping the sign from the projection parallel to the sliding direction. However,

²The uncertainty Δy is calculated as $\Delta y = \left| \frac{\partial y}{\partial x} \Delta x \right|$ for uncertainty Δx and $y(x)$

we omit such compromises as this might make analysis interpretation more difficult, and we use only the parallel component going forward.



(a) Decomposition into group inner sheet (sheet) and pull blocks (PB). (b) Decomposition into parallel (F_{\parallel}) and perpendicular (F_{\perp}) to drag sliding direction.

Figure 1.3: Friction force decomposition on the data shown in figure 1.1 with applied savgol filters similar to that of figure 1.1b with window polyorder 5 and window length of 150 timesteps (corresponding to a sliding distance of 3 Å or a time window of 15 ps).

1.2.3 Center of mass path

From the previous observations of the friction force time series we see evidence of a stick-slip behaviour. Specially, we see in figure 1.3b that this might be the case both parallel and perpendicular to the sliding direction. By looking at the x, y -position for the sheet center of mass (COM) we observe the stick-slip motion manifested as a variation in COM speed combined with a side to side motion as shown in figure 1.4a. In an attempt to increase the magnitude of the slips we evaluate a similar simulation with spring constant $K = 30 \text{ N/m}$ (see figure 1.4b) in contrast to that of an infinite spring constant. While the maximum slip speed stays within a similar order of magnitude the slip length in the sliding direction is increased along with the side to side motion. Note that the axis scale is different between figure 1.4a and 1.4a. However, in both cases we observe that the side to side motion is associated with a low speed, meaning that is more reminiscent of a “slow” creep alignment with the substrate than a slip.

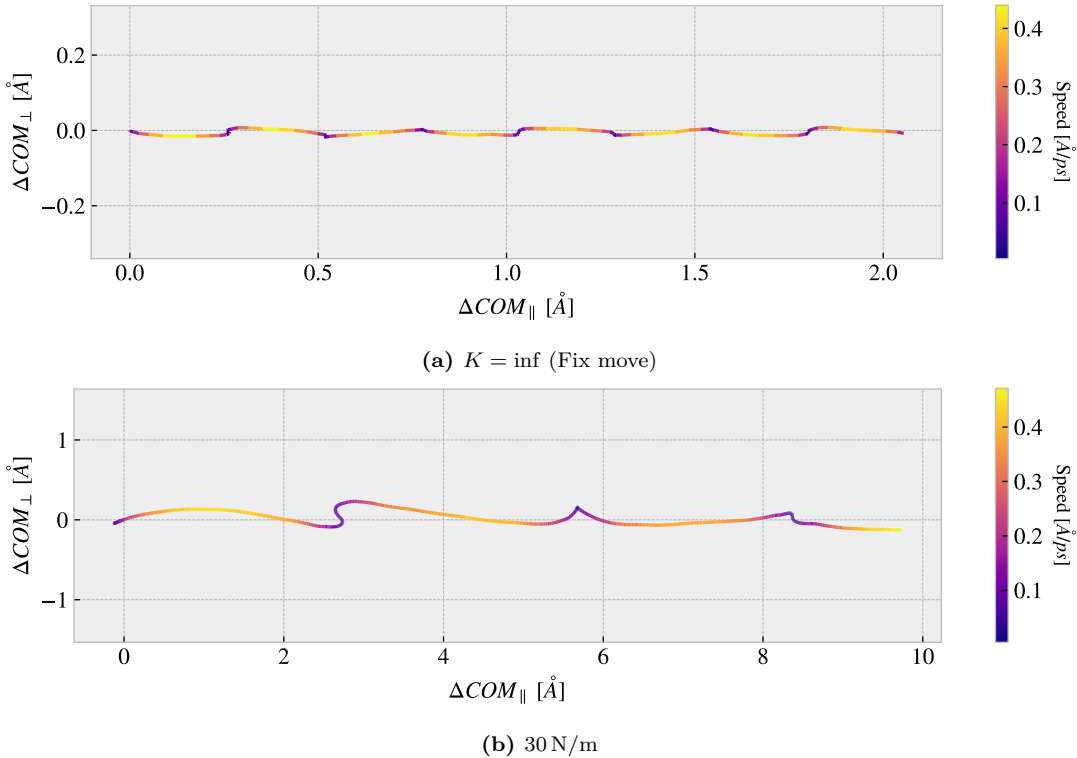


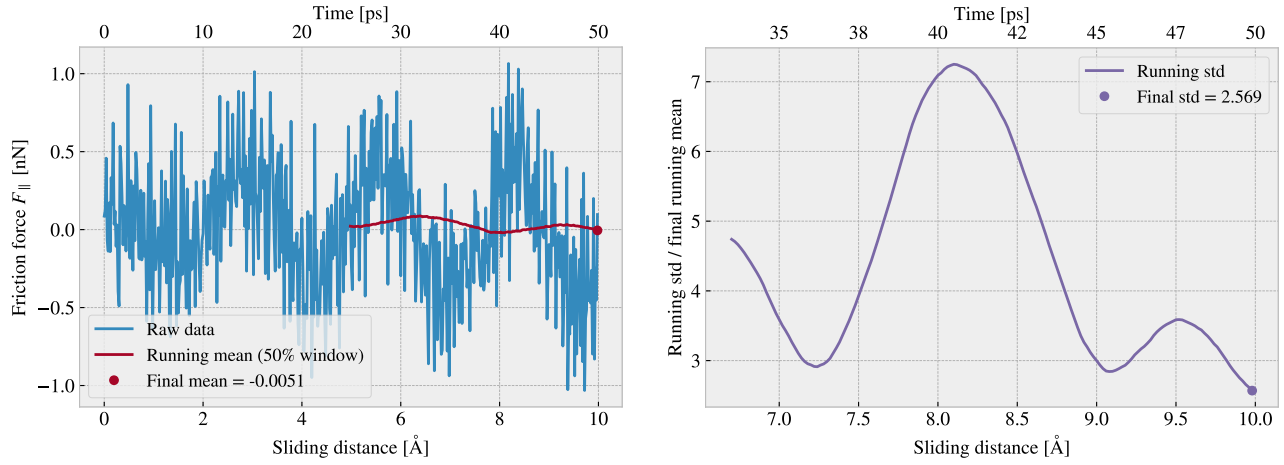
Figure 1.4: Center of mass position relative to the start of the sliding phase in terms of the direction parallel to the sliding direction ΔCOM_{\parallel} and the axis perpendicular to the sliding direction ΔCOM_{\perp} . The colorbar denotes the absolute speed of the COM.

1.3 Defining metrics for dynamic and static friction

In order to evaluate the frictional properties of the sheet we reduce the comprehensive friction force time series addressed in section 1.2 into single metrics describing the dynamic and static friction. The natural choice is to use the mean and max values of the time series.

1.3.1 Dynamic friction

For the dynamic friction measurement we take the mean value of the latter half of the dataset to ensure that we are sample from a stable system. For a full sliding simulation of 400 Å we thus base our mean value on the latter 200 Å of sliding. In figure 1.5a we have shown the friction force of the first 10 Å of sliding together with a running mean with window length of 5 Å corresponding to 50% the data length. This is merely done to illustrate the sampling procedure and by only using a 10 Å sliding distance the final mean estimate (indicated with a dot) takes a negative value due to the specific cut-off of the few oscillations captured here. Nonetheless, one approach to quantify the uncertainty of the final mean estimate is to consider the variation of the running mean preceding the final mean value. The more the running mean fluctuates the more uncertainty associated with the final estimate. However, only the running mean “close” to the ending should be considered, since the first part will rely on data from the beginning of the simulation. From the Fourier analyse in section 1.2.1 we found the longest significant oscillation period to be $\sim 71 \text{ \AA}^{-1}$ corresponding to $\sim 35\%$ of the running mean window consisting of 200 Å of slifing when including all the data. Hence, we use the standard deviation of the final 35% of the running mean to approximate the uncertainty of the final mean value, and we estimate the relative error by dividing the standard deviation by the final mean value. In figure 1.5b we showcase a running standard deviation of a window length 35% the running mean window in figure 1.5a for the illustrative case of a total 10 Å slide. The final uncertainty value is marked by a dot, and we see as expected that we get a high relative error of $\sim 257\%$ which corresponds well with the short sampling period and the mean value taking an unphysical negative value.



(a) Running mean with window length 5 Å (50% the data length). (b) Running std with window length 1.75 Å (35% the mean window length.)

Figure 1.5: Running mean and running standard deviation (std) on the friction force data from a 10 Å of sliding simulation. The running mean window is 50% the data length while the running std window is 35% the running mean window length.

When including the full dataset of 400 Å of sliding, such that std window actually matches with the longest period of oscillations expected from the data, we get a final relative error of $\sim 12\%$ as shown in fig 1.6. This is arguable just at the limit for an acceptable error, but as we shall see later (Make a reference to fig or sec) this high relative error is mainly connected to the cases of low friction. When changing the simulation parameters, such that the mean friction evaluates to considerable higher values, the relative error drops to the order (put in numbers). One interpretation of this finding is simply that the oscillations in the running mean is somewhat independent of the magnitude of the friction. In that case, the relative error will spike for the low friction cases.

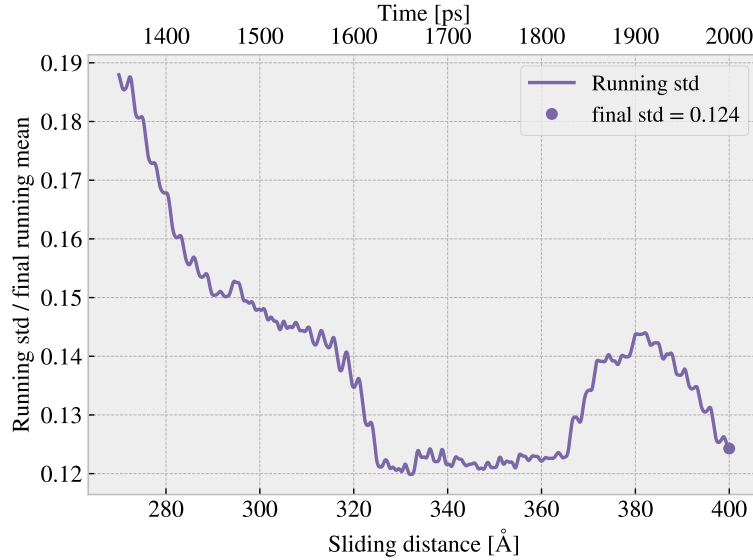


Figure 1.6: Running standard deviation (std) for a full 400 Å sliding simulation. The running std window is 70 Å (35% the running mean window of 50% the data length).

1.3.2 Static friction

The max value is the most obvious choice for addressing the static friction, even though that the definition of the static friction is a bit vague. When considering the friction force time series in figure 1.1 we observe that

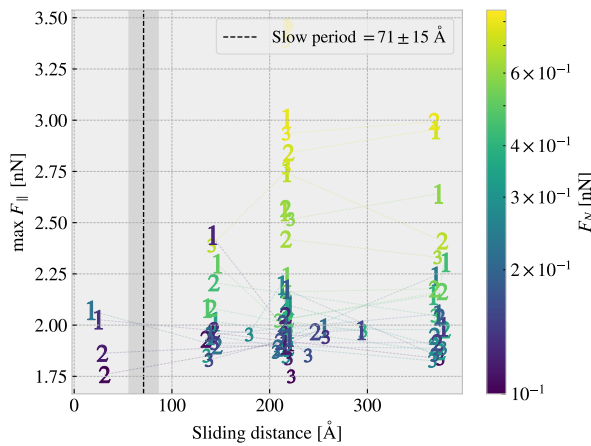


Figure 1.7: Distribution of top three max friction force peaks for 30 uniformly sampled normal forces $F_N \in [0.1, 10]$ nN. The dotted line and the grey area marks the slowest significant oscillation period found in the data and thus marking a dividing line for whether a peak falls within the “beginning” of the sliding simulation.

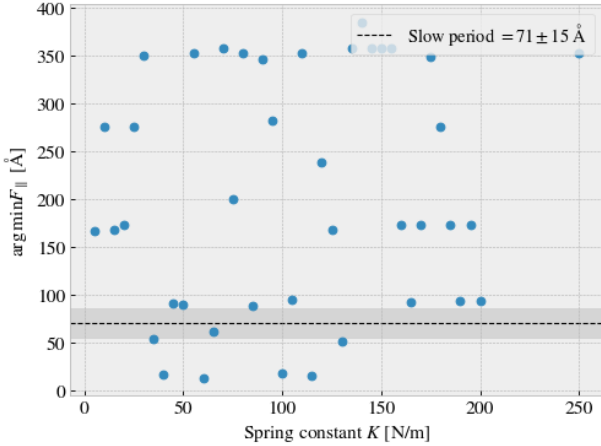


Figure 1.8: Sliding displacement for the max friction peak to appear as a function of spring constant. Fixmove is tmp mapped to $K = 200$ here without any discontinuous lines.

the stick-slip oscillations increase in magnitude toward a global peak at ~ 20 Å. Thus, we could identify this peak as the static friction force, but the global max does in fact rarely fall within the first part of the sliding. In figure 1.7 we investigate the top three max value, at which sliding distance they occur and at what magnitude, for 30 uniformly sampled normal forces in the interval [0.1, 10] nN. It is immediately clear that only few of the peaks falls within the “beginning” of the simulation defined by the slowest significant oscillation period of 71 ± 15 Å. In fact only 2/30 global values and 4/90 top three values can be associated to the start of the sliding by this definition. Thus, this result suggest that the max value cannot be used as a reliable measure for the static friction either due to its lack of presence or due to the simulation setup procedure. For a more typical evaluation of the static friction force one would increase force slowly until the first slip significant slip is recorded (a series of precursors is expected to precede this). In our simulations we drag the sheet relatively fast in a rigid manner which might be the reason for the lacking the static friction. Bonelli et al. [1] reported that the stick-slip behaviour was only presented when using a relatively soft spring. Thus, by changing the spring constant we investigate possibility to observe a static friction (**I kind of interchanged stick-slip and static friction int his argument, but I still think it can be used to argue for doing the test...**) response within the framework of our simulation procedure as shown in figure 1.8. However, the results do not indicate any implications that a recognizable domain exist for which the static friction response would be reliable. Hence, we will base the final assessment on frictional properties purely on the dynamic friction force.

1.4 Out of plane buckling

The out of plane buckling is the main motivation for applying the kirigami inspired cuts to the sheet. Thus, we perform a stretch simulation in a low temperature $T = 5$ K vacuum in order to verify that the chosen cut configurations do in fact contribute to a significant out of plane buckling when stretched. For the non-cut, popup and honeycomb configuration we assess the movement in the z-direction (perpendicular to the plane) during the stretch, which we visualize by the min and max z-value along with the atom count quartiles 1%, 10%, 25%, 50% (median), 75%, 90% and 99% as shown in figure 1.9. We observe that the popup and honeycomb pattern buckles considerable out of plane during the stretch in comparison to the non-cut sheet which only exhibit minor buckling of ~ 2 Å which is on the same order as the atomic spacing in the sheet. We also notice that the popup pattern buckles more in consideration to the min and max peaks while the 1%, 99% quartiles is on the same

magnitude as the honeycomb. By looking at the simulation visualization (**include OVITO figures for vacuum stretch as well?**) we can conclude that this is mainly due to the fringes of the sheet “flapping” around.

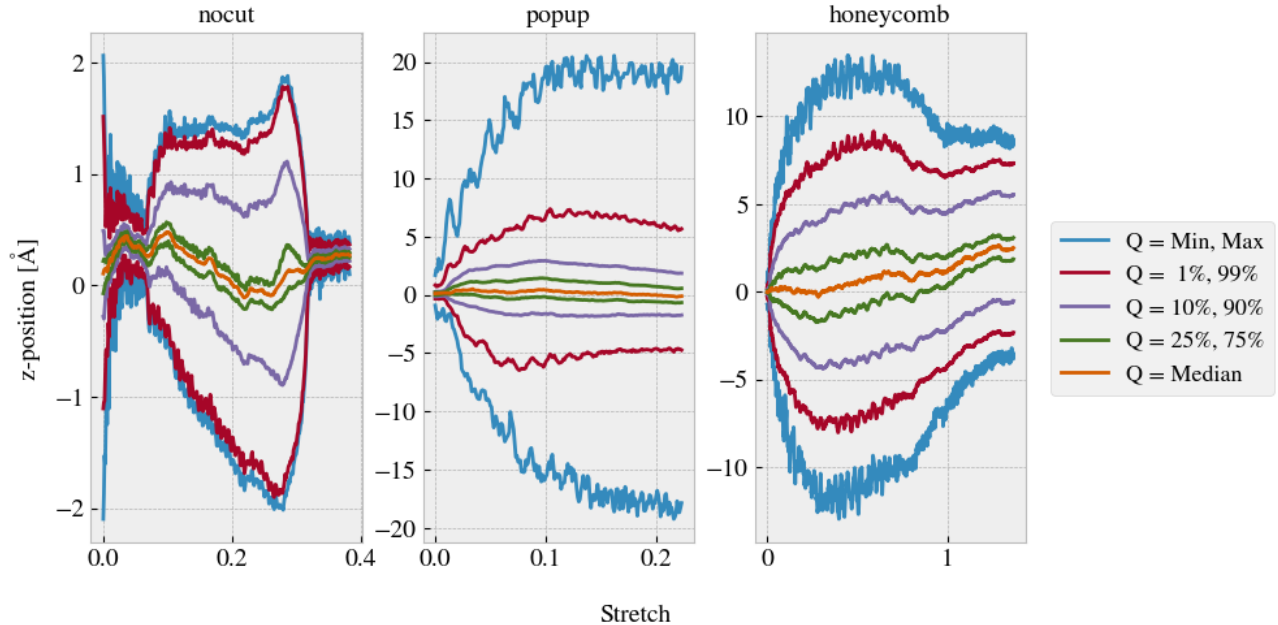


Figure 1.9: Out of plane buckling during stretch of sheets in vacuum at $T = 5$ K. Reading from left to right the vacuum rupture stretch are 0.38, 0.22 and 1.37. **perhaps use a color scale instead of the standard color cycles here.**

The next step is to verify that the buckling will lead to a significant altering of the contact area when the sheet is in put in contact with the substrate. We investigate this by simulating the stretch at the default temperature $T = 300$ K with the presence of contact forces between the sheet and substrate. Note that no normal load is applied as the sheet and substrate is sufficiently attracted by the LJ potential. Selected frames from the simulation is shown in appendix ???. We assess the contact area by the relative amount of atoms in the sheet within chemical range of the substrate. The cut-off for this interaction is 4 Å corresponding to $\sim 120\%$ the LJ equilibrium distance. Since the contact area is usually calculated as the amount of atoms in contact multiplied with an associated area for each contact this feature is taken to be proportional to the contact area. The relative amount of bonds as a function of stretch for the various configurations is shown in figure 1.10 which clearly indicates a drop in contact area as the cutted sheets are stretched.

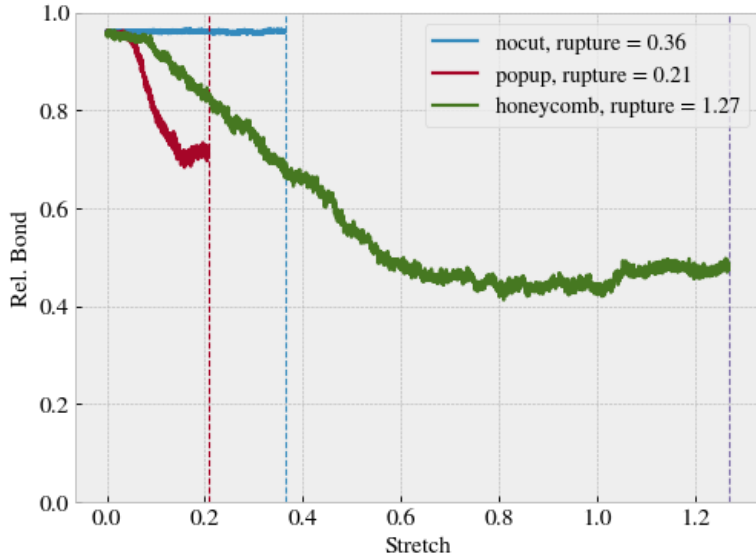


Figure 1.10: Contact vs. stretching of the sheet, where the contact is measured by the relative amount atoms in the sheet within chemical interaction range to the substrate. The cut-off for this interaction range is 4 Å corresponding to $\sim 120\%$ the LJ equilibrium distance. $T = 300$ K

Compare figure 1.10 to that of figure 1.15 where multiple simulations constitute the stretch-contact curve.

1.5 Investigating selected parameters

We investigate the importance of the physical variables T , v_{slide} and K (make plots for scan angle as well?) and the choice of timestep dt . This is done partly understand how the dependencies relate to theoretical, numerical and experimental results, and partly to understand how these parameter choices defines the regime for our multi configurational search. We use the default parameters in table 1.2 with exception of the single parameter of interest which is varied in a reasonable range of the default choice. In figure 1.11-1.14 the dynamic friction estimate and the max friction force is shown as a function of T , v_{slide} , K and dt respectively. For the dynamic friction estimate the absolute error is denoted by a shaded error which linearly connects the points.

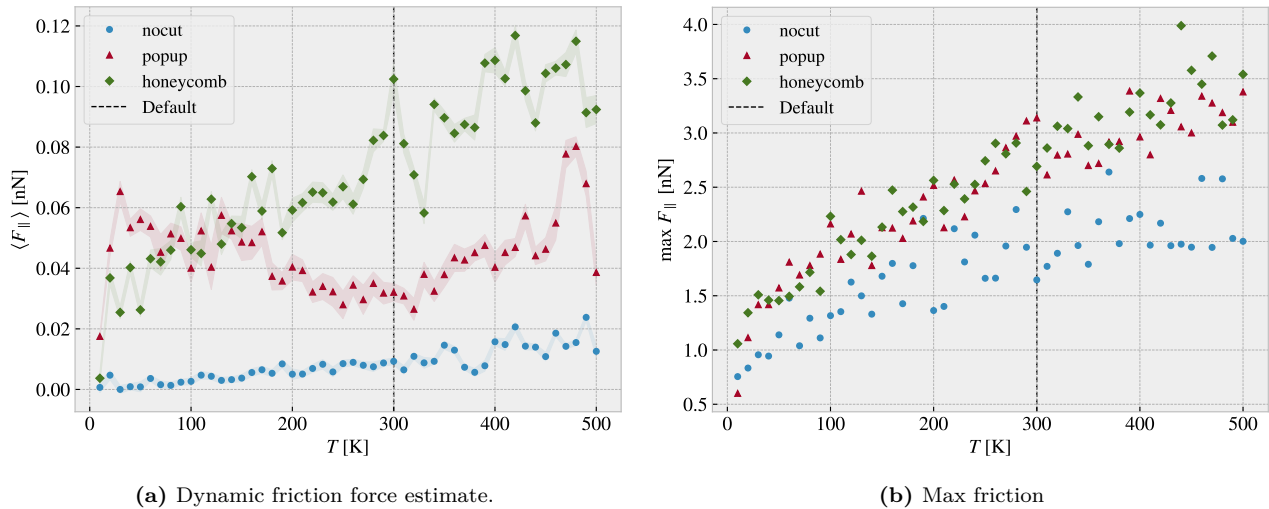


Figure 1.11: Temperature.

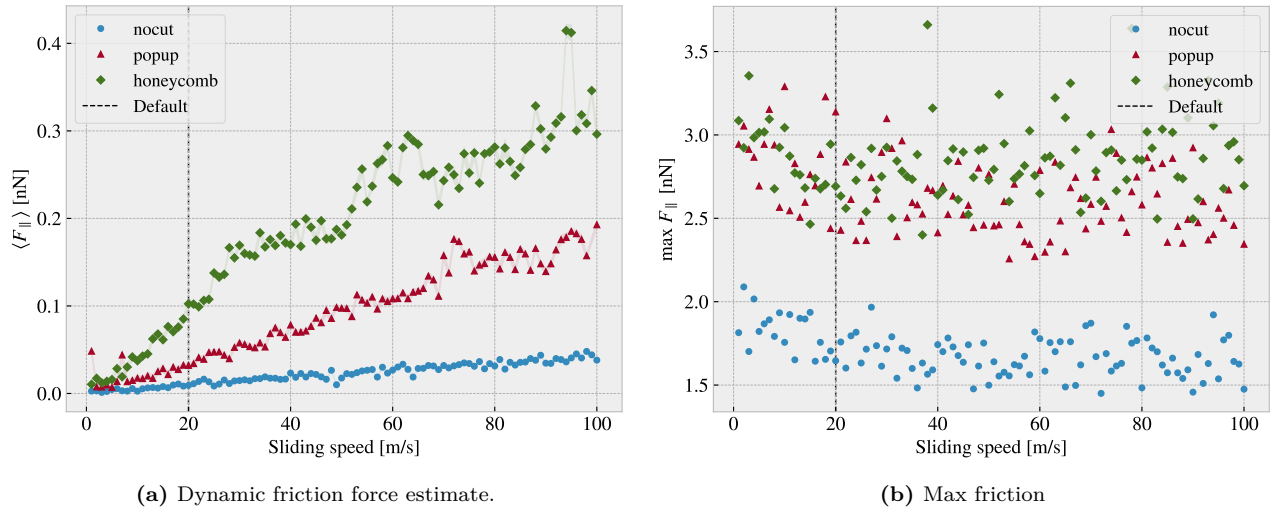


Figure 1.12: Sliding speed

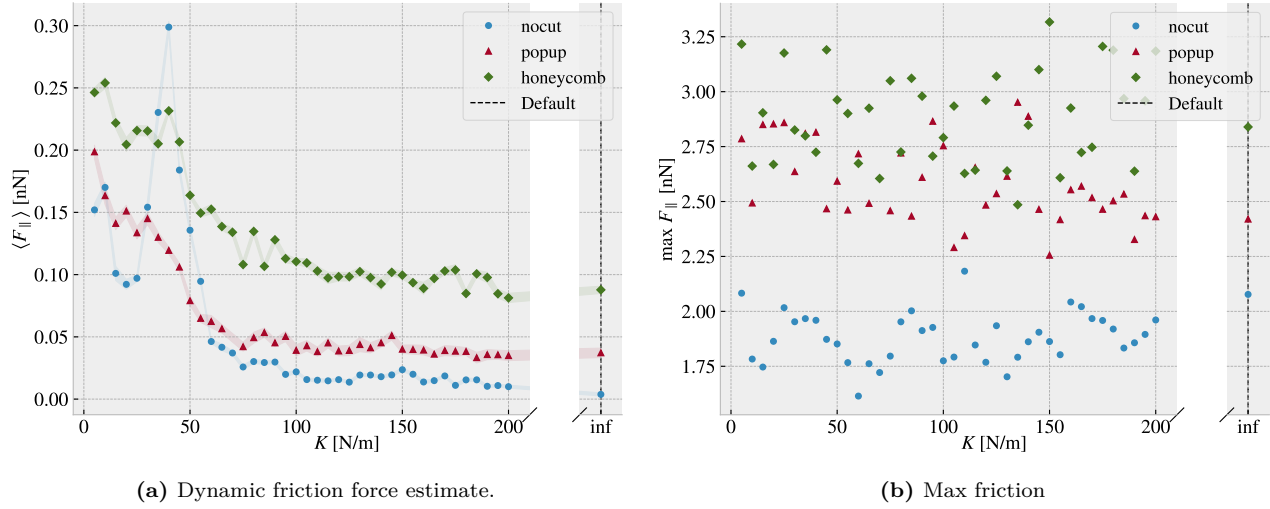


Figure 1.13: Spring constant

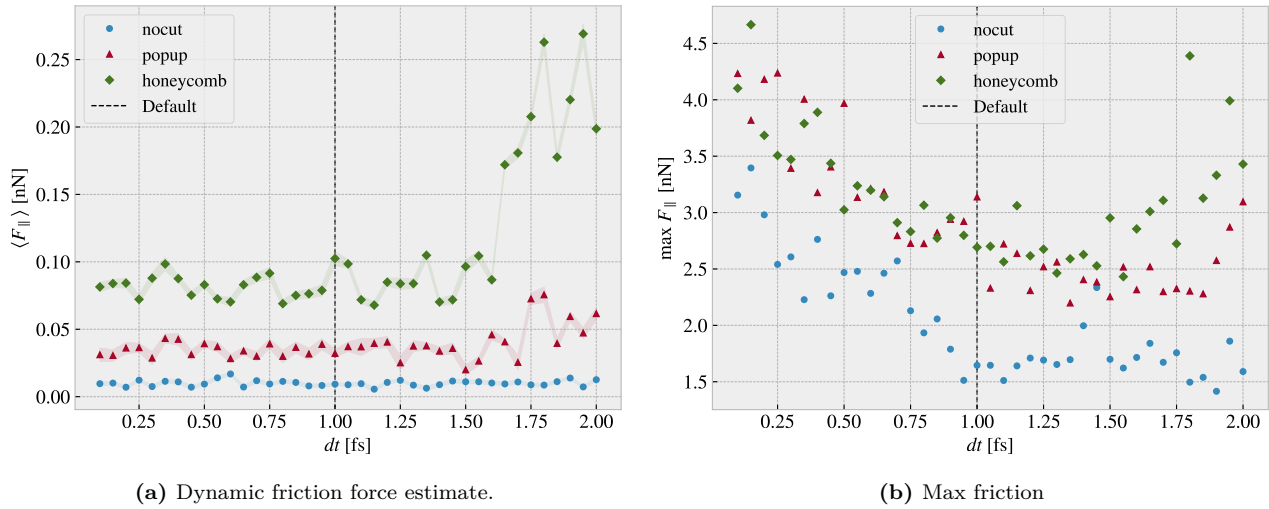


Figure 1.14: Timestep

Quick thoughts:

- Temperature: We do clearly not see the $1/T$ temperature decrease. The non-cut sheet seems to showcase a linear relationship which is also somewhat present for the honeycomb which matches some of the findings in other MD simulations. For the popup we do see a local decrease at low temperatures which flip at around the default $T = 300$ K temperature. The max friction peaks seem to increase with temperature as well indicating that the peaks might be associated with thermal fluctuations rather than actual stick-slip behaviour. This supports the finding that the static friction response is not significantly present in these simulations.
- Velocity: Considering the non-cut sheet first the velocity dependency is seemingly linear which deviates from the expected logarithmic trend. For the cutted configurations we find some peaks which might indicate the presence of resonance frequencies. The cutted sheet might be closer to a logarithmic trend, but this is not spot on either. The max friction seems to decrease slightly with small velocities and then stay rather constant. This can probably be explained by the reduced time to stick between stick-slip.
- Spring constant: On all three configurations the dynamic friction decreases with an increasing spring constant. The best explanations might be due to the lack of freedom to “get stuck” in incommensurable configurations. We also notice that the friction varies a lot at lower spring constants supporting the choice of having a stiff spring for stability reasons. Especially the non-cut sheet peaks at $K = 40$ N/m. The max friction seem to be constant with K .
- dt : The dynamic friction is relatively stable around the default choice of $dt = 1$ fs. However, the fluctuations with respect to dt is more significant for popup pattern and even more for the honeycomb pattern. This indicates that the more complex dynamics of the simulation is more sensitive to the timestep. We might interpret this information as an additional measure of uncertainty. The maximum friction decreases with increasing timestep which can be asserted a statistical interpretation: Higher peaks will be captured by the high resolution of a low dt and vice versa. The high max values towards the point of $dt = 2$ fs is most likely due to the approach of instability in the simulation as seen more clearly for the dynamic friction evaluation.

1.6 Normal force and stretch dependencies

Till this point we have only changed variables one by one to investigate single dependencies. We now advance the study to a simultaneous variation of stretch and normal force.

Explain how the stretch is uniformly sampled within equally divided intervals and the normal force is actually uniformly sampled in a given range. Argue that the first might be approximately uniformly distributed for large numbers.

Talk about rupture test also. Maybe in the theory/method section under numerical procedure: Before simulating a rupture test is perform to determine under what stretch the sheet ruptures. This is a slightly higher threshold than when applied normal load and sliding along the substrate.

1.6.1 Contact area

??

We reproduce the contact area investigation of figure 1.10 with the modification that the contact count is measured as an average of the latter 50% of the sliding simulation at a non-zero applied normal load. The results are shown in figure 1.15 with 30 attempted (some rupture) stretch (pseudo) uniformly distributed stretch between 0 and the rupture point and 3 uniform distributed normal loads in the interval [0.1, 10] nN.

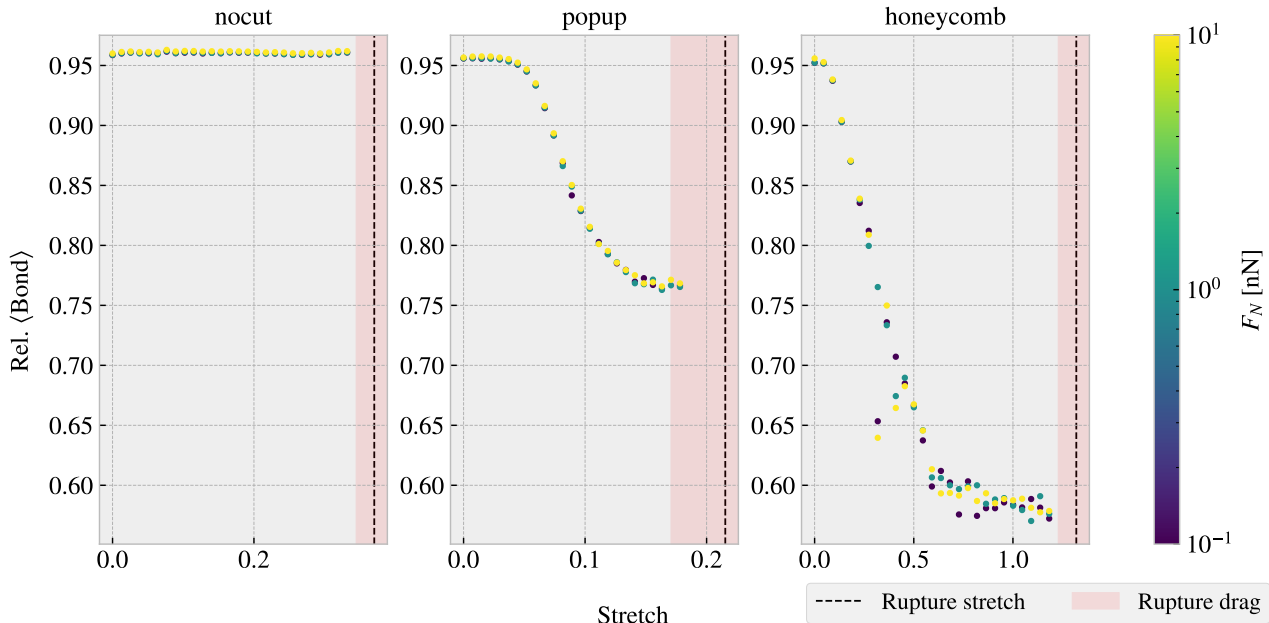


Figure 1.15: Average relative amount of bonds between the sheet and the substrate defined by the cut-off distance of 4 Å. The average is taken over the latter half of the sliding phase. The red shade denotes the stretch range where ruptures occur at certain normal loads under sliding while the black-dotted line represents the rupture point due to stretching (rupture test)

From figure 1.10 we observe a significant decrease in the contact due to stretching of the cut configurations in contrast to the non-cut which stays roughly constant. This is reminiscent of the non-sliding stretch vs. contact curve shown in figure 1.10. Given these results, theoretically one would expect the dynamic friction to decrease with stretch for the cut configurations.

1.6.2 Stretch

We make a similar analysis as done in the previous section ?? with the substitution of friction force instead of contact (The data is taken from the same simulations runs). The dynamic friction force (put uncertainty here even though that it is quite low?) and the max friction is shown in figure 1.16a and 1.16 respectively.

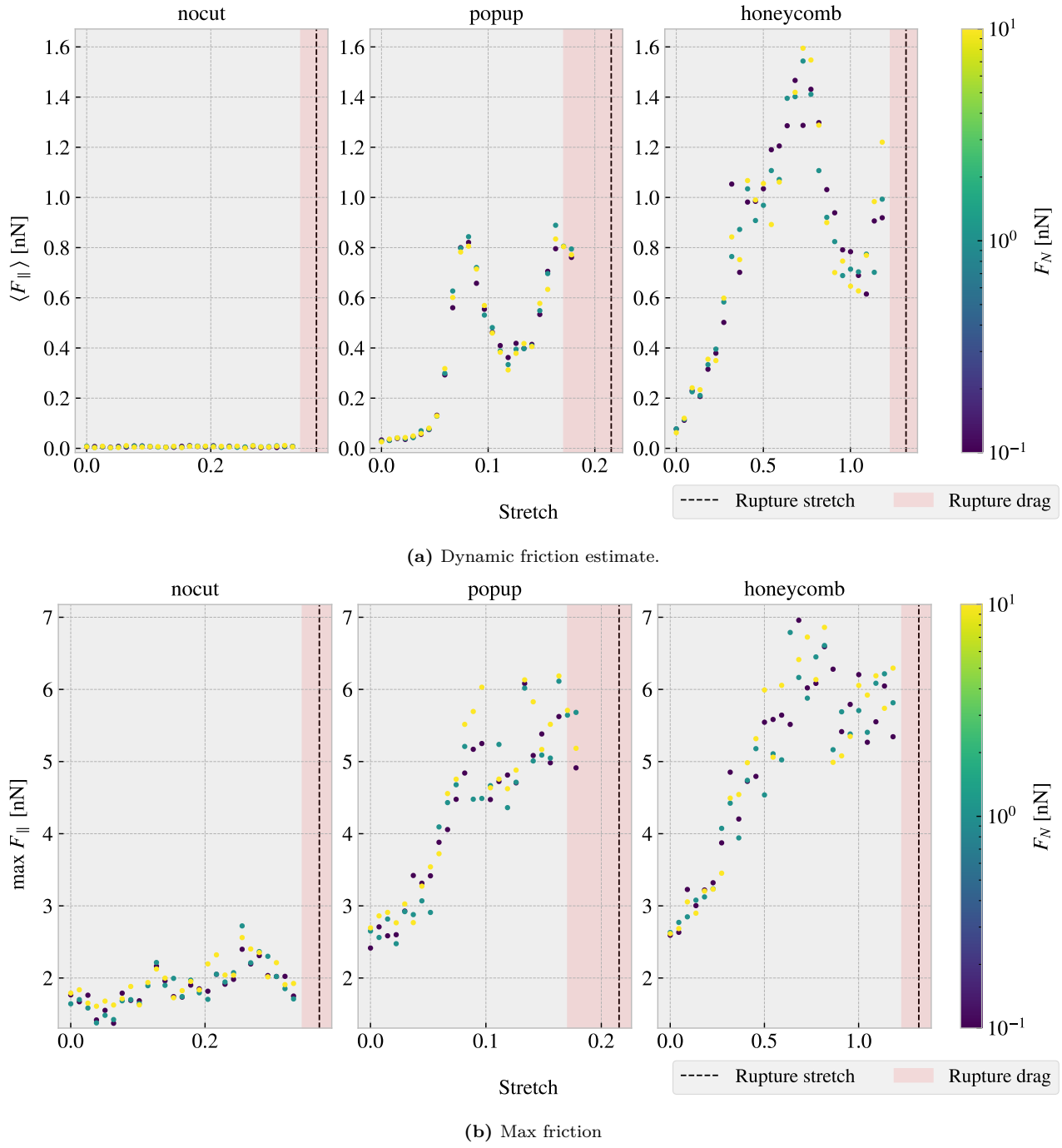


Figure 1.16: CAPTION

From figure 1.16a we find to our surprise that the dynamic friction increase with stretch for the cut configurations despite a simultaneous decrease in contact area as shown in figure 1.15. This suggests that the amount of chemical bonding atoms is not the dominant mechanism for the friction of this system. Instead, we might point to a mechanism more mechanical of nature associated to phonon excitations. When the cut sheet is stretched the stress (show stress maps somewhere or not necessary?) might induce a certain distribution and magnitude of point pressures to favor energy dissipation. Nonetheless, the results showcase a strong coupling between stretch and friction force, also for the max friction force, which is beyond the expectations at this stage of the study. The non-cut configuration does not show significant dependency on the stretch which reveal that this effect is only present when combining cut and stretch and not purely by stretching the sheet.

By considering the increase in dynamic friction towards the first peak we get a relative friction increase and increase vs. stretch ratios as described in table 1.3. While the honeycomb force increase towards the first peak is approximately linear the popup exhibits seemingly exponential growth which yield a slope on the order ~ 30 nN.

Table 1.3: (stretch, dynamic friction) coordinates from figure 1.16a at start and the first peak respectively used to approximate the relative increase in friction force and the ratio for friction increase vs. stretch for sait range. In practice the latter ratio denotes the slope of a forced linear trend.

Configuration	Start	First peak	Relative increase	Friction force vs. stretch ratio [nN]
Popup	$\sim (0, 0.03)$	$\sim (0.082, 0.83)$	27.7	9.76
Honeycomb	$\sim (0, 0.07)$	$\sim (0.728, 1.57)$	22.4	2.06

Additionally, we notice that both the popup and honeycomb also exhibits stretch ranges where the dynamic friction force decrease with increasing stretch. Qualitatively we assign the slope to be on the same order of magnitude as those towards the first peak. This is useful for the prospect of taking advantage of this phenomena as we can essentially achieve both higher and lower friction for increasing stretch for different starting points.

1.6.3 Normal force

Main take away from this section should be that the normal force does not really change the friction much; The friction coefficient is extremely low, but I'm not sure how well the linear fits are (whether they are linear or sublinear). Not sure if I should do a linearly increasing normal force for better linear plots?

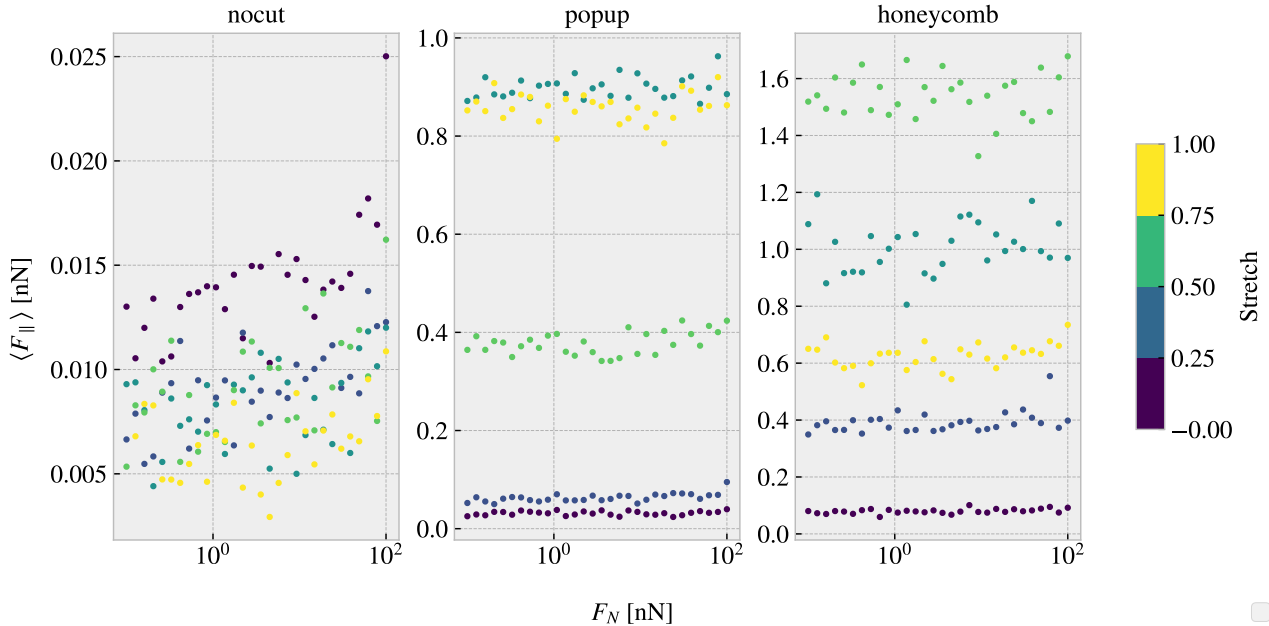


Figure 1.17: ...

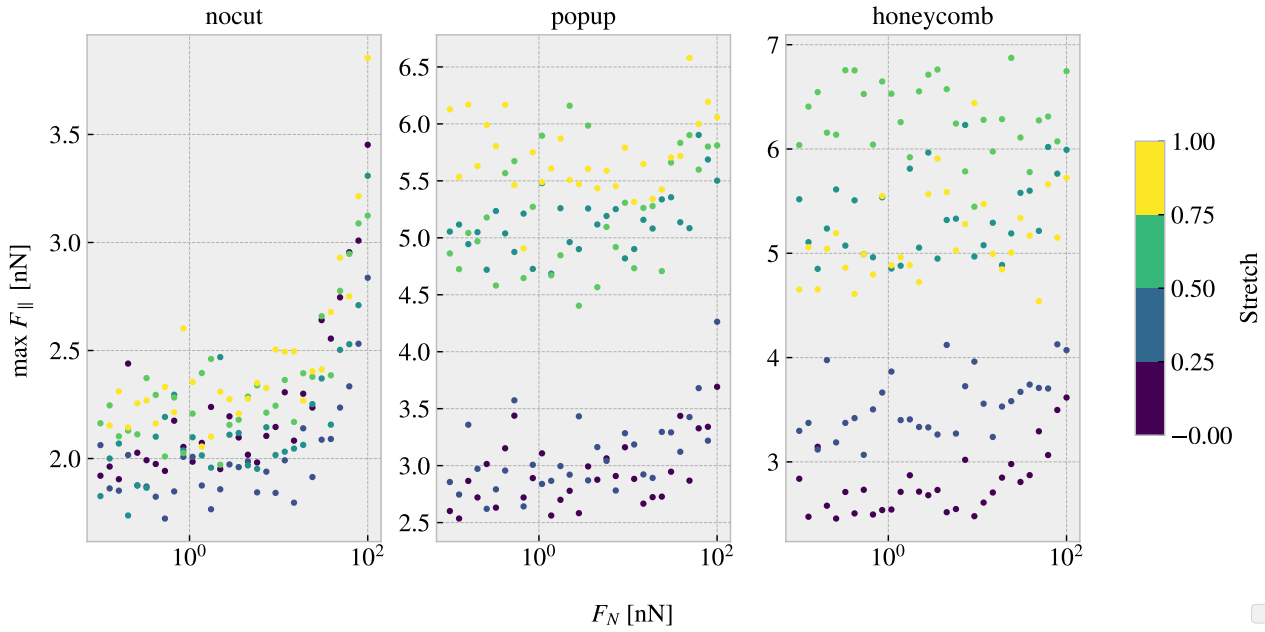


Figure 1.18: Colorbar is only fitted for the right plot (honeycomb)... this should be fixed. Should I have run a linear distribution of FN so I could plot it linear here also...?

Table 1.4: Mean friction coeff

nocut	$0.00009 \pm 1 \times 10^{-5}$	$0.00005 \pm 1 \times 10^{-5}$	$0.00004 \pm 1 \times 10^{-5}$	$0.00005 \pm 2 \times 10^{-5}$	
popup	$0.00005 \pm 3 \times 10^{-5}$	$0.00024 \pm 5 \times 10^{-5}$	$0.0002 \pm 2 \times 10^{-4}$	$0.0005 \pm 1 \times 10^{-4}$	$0.0003 \pm 2 \times 10^{-4}$
honeycomb	$0.00013 \pm 6 \times 10^{-5}$	$0.0006 \pm 3 \times 10^{-4}$	$0.0004 \pm 6 \times 10^{-4}$	$0.0007 \pm 6 \times 10^{-4}$	$0.0009 \pm 3 \times 10^{-4}$

Table 1.5: Max friciton coeff

nocut	$0.0139 \pm 9 \times 10^{-4}$	$0.0083 \pm 7 \times 10^{-4}$	$0.010 \pm 1 \times 10^{-3}$	$0.0105 \pm 9 \times 10^{-4}$	
popup	$0.007 \pm 2 \times 10^{-3}$	$0.010 \pm 2 \times 10^{-3}$	$0.007 \pm 2 \times 10^{-3}$	$0.009 \pm 3 \times 10^{-3}$	$0.006 \pm 2 \times 10^{-3}$
honeycomb	$0.010 \pm 1 \times 10^{-3}$	$0.007 \pm 2 \times 10^{-3}$	$0.007 \pm 3 \times 10^{-3}$	$0.000 \pm 3 \times 10^{-3}$	$0.004 \pm 3 \times 10^{-3}$

One theory for the low friction coefficient might depend on the fact that the normal force is only applied on the pull blocks. Especially with the cut sheet the tension drops such that the effective normal force on the inner sheet is not changing very much. By this theory the friction force vs. normal force on the pull blocks should look a bit more like expected and we might make some plots of those to check

When looking at the graphs for the PB the max friction is visually textbook linear, while the mean friction is a bit more linear but also with negative coefficients...

1.7 Computational cost

Talk about the computational cost of different choices. How does computation time scale with drag speed, dt and maybe T and K as well. One could also mention scaling with system size.

Show how the number of cores per simulation scale to argue that running on just one core (maybe 4) is smart for the next step of many simulations.

Mention the trouble with GPU to show that this was considered, and in fact this was the reason for choosing the Tersoff potential over the AIREBO which is perhaps more common these days...

Chapter 2

Dataset study

2.1 Generating data

We generate the dataset by simulating various sheet cut configurations under multiple combinations of normal load and stretch. For each configuration we sample 15 pseudo uniform (refer to relevant section here) stretch values between zero and the rupture stretch found in the rupture test. The normal force is uniformly sampled in the range $[0.1, 10]$ nN. In total this gives 3×15 data points for each configuration. For the remaining parameters we use the values presented in the pilot study (see table 1.1). We generate 68 configurations of the Tetrahedron pattern type, 45 of the Honeycomb type and 100 of the Random walk type which is shown in Appendix C?. A summary of the data points is given in table 2.1. The table shows that not all submitted data points “makes it” to the final dataset. This is due to the combination of our numerical procedure and small variations in the rupture stretch point. After performing the rupture test the simulation is restarted with a new substrate size corresponding to the measured rupture stretch limit and also with new random velocity and thermostat initializations values. The sheet is then stretched and checkpoints of the simulation state (LAMMPS restart files) are saved for each of the targeted stretch samples. However, if the rupture points arrives slightly early than suggested by the rupture test, some sampled stretch values might not get a corresponding checkpoint file. Thus, these data points are not included in the data set even though they ideally should have been noted as a rupture event. This could quite easily have been mitigated by a rewrite of that part of the code, but it was first discovered after the dataset had been created. However, the dataset still includes 11.57 % rupture events and it is most likely that the most cases with a lost rupturer event have a rupture event stored for the preceding stretch value instead which captures the information of the sheet stretch limit on its own.

Table 2.1: Summary of the number of generated data points in the dataset. Due to slight deviations in the rupture stretch and the specific numerical procedure not all submitted simulations “makes it” to the final dataset. Notice that the Tetrahedon (7, 5, 2) and Honeycomb (2, 2, 1, 5) from the pilot study is rerun as a part of the Tetrahedon and the Honeycomb datasets separately. In the latter datasets the reference point for the pattern is randomized and thus these configurations is not fully identical. This is the idea behind the difference of 2 in the total sum.

Type	Configurations	Submitted data points	Final data points	Ruptures
Pilot study	3	270	261	25 (9.58 %)
Tetrahedon	68	3060	3015	391 (12.97 %)
Honeycomb	45	2025	1983	80 (4.03 %)
Random walk	100	4500	4401	622 (14.13 %)
Total	214 (216)	9855	9660	1118 (11.57 %)

2.2 Data analysis

In order to gain insight into the correlations between variables associated to the simulations we calculate the correlations coefficients between all variable combinations. More specific, we are going to calculate the Pearson

product-moment correlation coefficient (PPMCC) for which is defined, between data set X and Y , as

$$\text{corr}(X, Y) = \frac{\text{Cov}(X, Y)}{\sigma_X \sigma_Y} = \frac{\langle (X - \mu_X)(Y - \mu_Y) \rangle}{\sigma_X \sigma_Y} \in [-1, 1]$$

where $\text{Cov}(X, Y)$ is the covariance, μ the mean value and σ the standard deviation. The correlation coefficients ranges from perfect negative correlation (-1) through no correlation (0) to a perfect positive correlation (1). The correlation coefficients is shown in figure 2.1

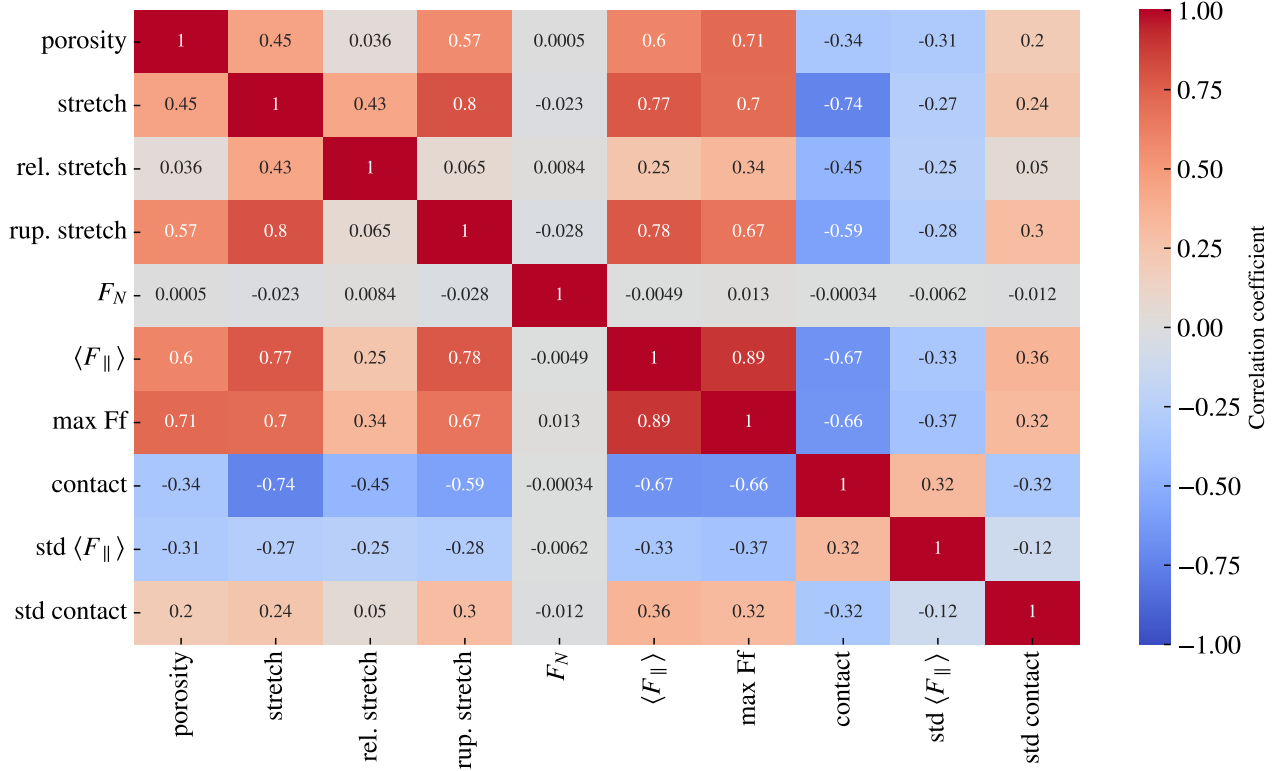


Figure 2.1: Pearson product-moment correlation coefficients for the full datset (see table 2.1).

From figure 2.1 we especially notice that the mean friction force $\langle F_{\parallel} \rangle$ has a significant positively correlation with stretch (0.77) and porosity (0.60) (void fraction). However, the relative stretch, which is scaled by the rupture stretch, has a weaker correlation of only 0.25 which indicates that it is the absolute stretch value that has the most significant impact on the friction force increase during stretching. This is further supported by the fact that the mean friction and the rupture stretch is also strongly positively correlated (0.78). From figure 2.1 we also observe that the contact bond count is negatively correlated with the mean friction (-0.67) and the stretch value (-0.74) which is consistent with the trend observed in the pilot study (figure 1.15 and 1.16a) of the contact decreasing with increasing stretch and mean friction. However, we must take note that the correlation coefficients is a measure of the strength and slope of a forced linear fit on the data. We clearly observed a non-linear relationship between stretch and mean friction for the tetrahedron and honeycomb pattern used in the pilot study (figure 1.16a) where the relationship was partwise characterized by a postive correlation for some stretch ranges and partwise negative correlation for other stretch ranges. Hence, interesting strong regime-specific correlations might not be accurately highlighted by the correlation coefficients shown in figure 2.1.

In figure 2.2 we have visualized the data (excluding the pilot study) for chosen pairs of variables on the axes. In addition to a visual confirmation of how the given correlations look in a 2D plot we also get a feeling for the coverage in various areas of the parameter space that we are eventually going to feed the neural network. The honeycomb pattern is spanning a significant larger range of stretch, contact and mean friction makes the data rather biased towards the Honeycomb pattern in those areas.

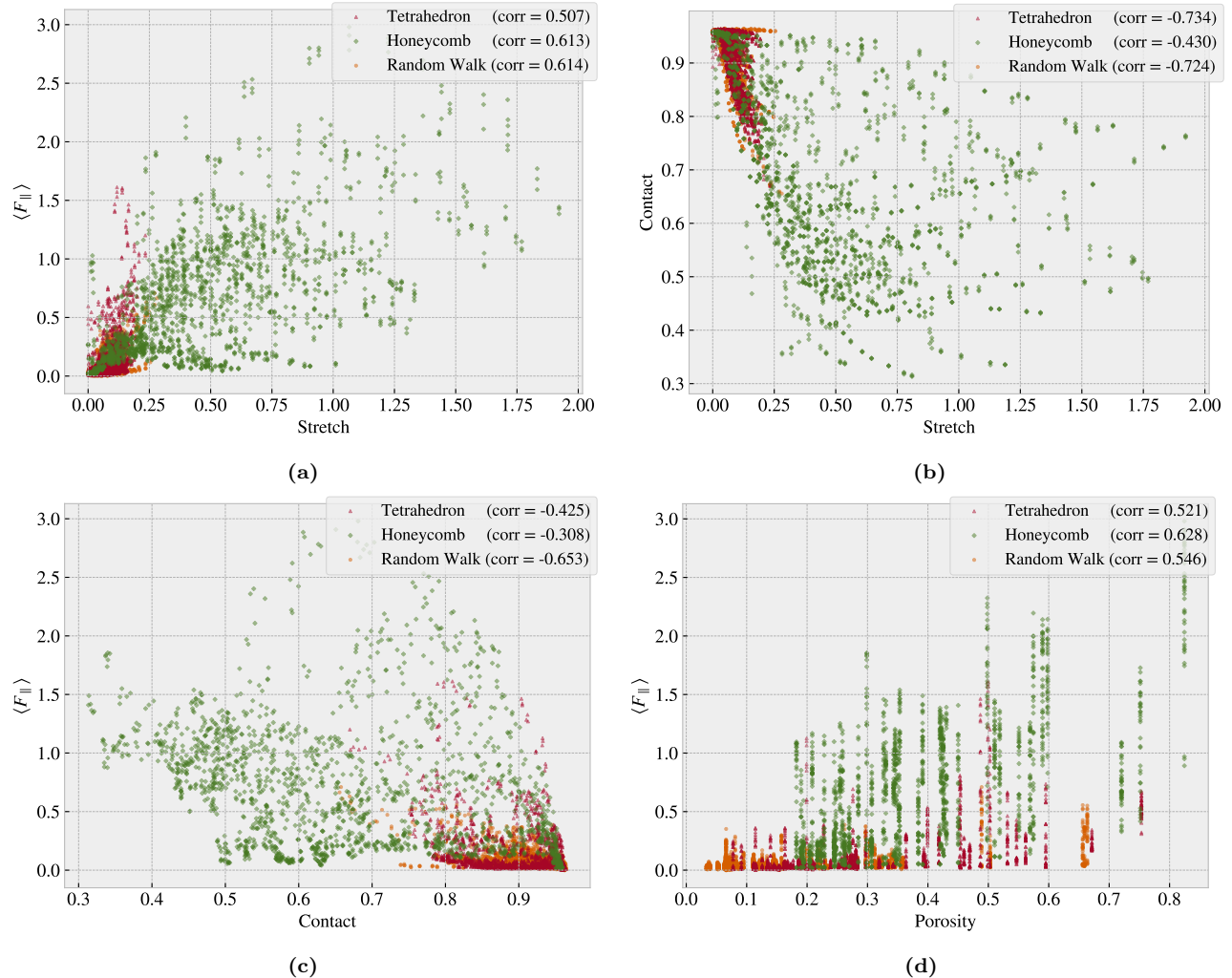


Figure 2.2: Scatter plot of the data sets Tetrahedron, Honeycomb and Random Walk (excluding the pilot study) for various variable combinations in order to visualize some chosen correlations of interest and distributions in the data

2.3 Properties of interest / Stretch profiles

Define somewhere that we will look at low friction, high friction and the biggest (forward) drop in friction corresponding to a significant negative friction coefficient.

Table 2.2: Interesting properties

Tetrahedron	Configuration	Stretch	Value [nN]
Min F_{fric}	(3, 9, 4)	0.0296	0.0067
Max	(5, 3, 1)	0.1391	1.5875
Max ΔF_{fric}	(5, 3, 1)	[0.0239, 0.1391]	1.5529
Max drop	(5, 3, 1)	[0.1391, 0.1999]	0.8841

Honeycomb	Configuration	Stretch	Value [nN]
Min F_{fric}	(2, 5, 1, 1)	0.0267	0.0177
Max	(2, 1, 1, 1)	1.0654	2.8903
Max ΔF_{fric}	(2, 1, 5, 3)	[0.0856, 1.4760]	2.0234
Max drop	(2, 3, 3, 3)	[0.5410, 1.0100]	1.2785

Random walk	Configuration	Stretch	Value [nN]
Min F_{fric}	12	0.0562	0.0024
Max	96	0.2375	0.5758
Max ΔF_{fric}	96	[0.0364, 0.2375]	0.5448
Max drop	01	[0.0592, 0.1127]	0.1818

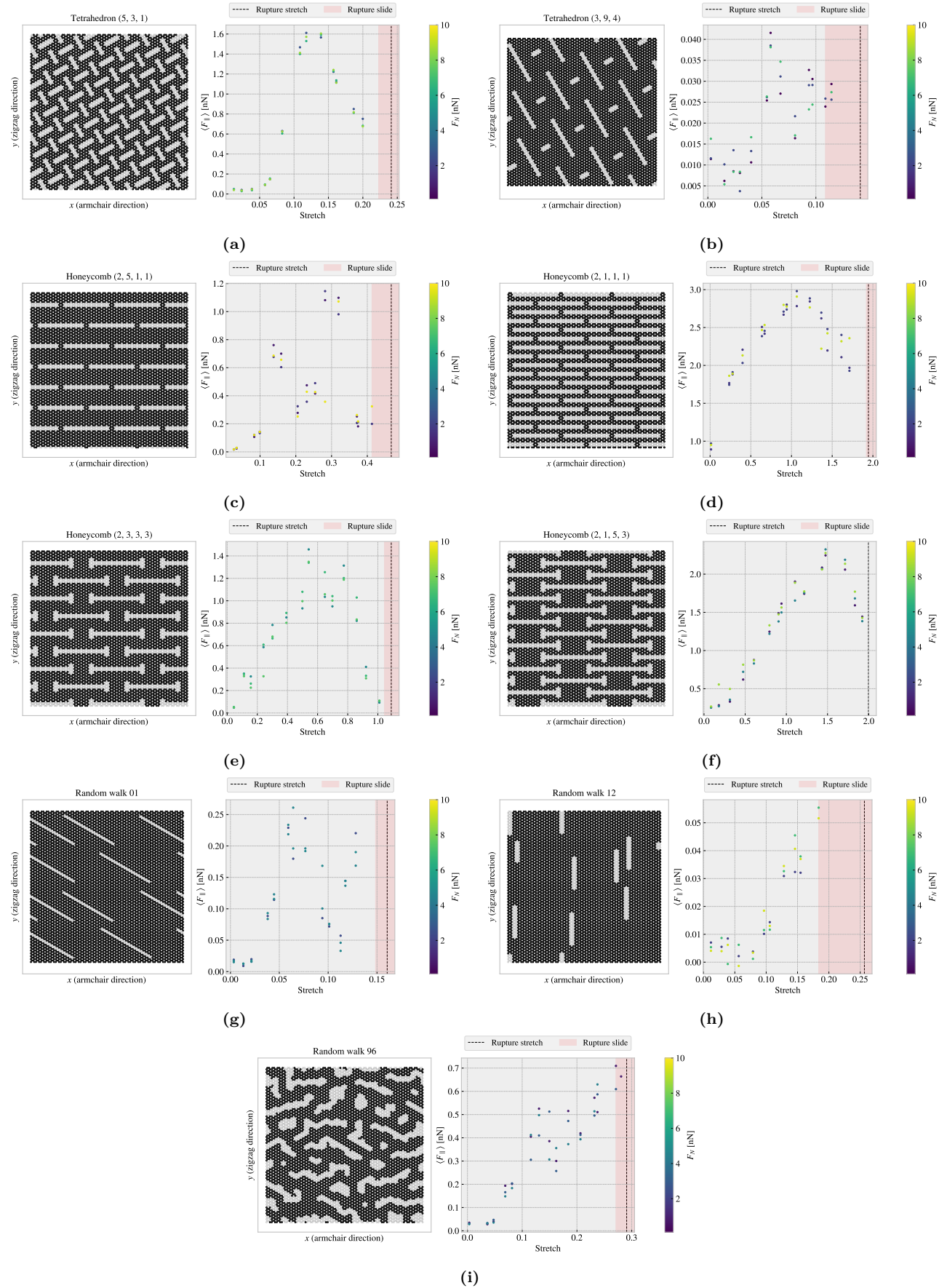


Figure 2.3

The stretch profiles for all the configurations are shown in appendix ??.

2.4 Machine learning

Staircase architecture tuning.

2.5 Accelerated Search

Having a network model that can predict friction force for a given configuration are able to search for some desired properties. Low and high friction and maximal negative friction coefficients

Here we pursue two different approaches for finding

1. Generate an enlarged dataset and run it through the ML model
2. Genetic algorithm

2.5.1 Markov-Chain Accelerated Genetic Algorithms

2.5.1.1 Talk about traditional method also?

2.5.1.2 Implementing for 1D chromosome (following article closely)

We have the binary population matrix $A(t)$ at time (generation) t consisting of N rows denoting chromosomes and with L columns denoting the so-called locus (fixed position on a chromosome where a particular gene or genetic marker is located, wiki). We sort the matrix rowwise by the fitness of each chromosome evaluated by a fitness function f such that $f_i(t) \leq f_k(t)$ for $i \geq k$. We assume that there is a transition probability between the current state $A(t)$ and the next state $A(t+1)$. We consider this transition probability only to take into account mutation process (mutation only updating scheme). During each generation chromosomes are sorted from most to least fitted. The chromosome at the i -th fitted place is assigned a row mutation probability $a_i(t)$ by some monotonic increasing function. This is taken to be

$$a_i(t) = \begin{cases} (i-1)/N', & i-1 < N' \\ 1, & \text{else} \end{cases}$$

for some limit N' (refer to first part of article talking about this). We use $N' = N/2$. We also define the survival probability $s_i = 1 - a_i$. In thus way a_i and s_i decide together whether to mutate to the other state (flip binary) or to remain in the current state. We use s_i as the statistical weight for the i -th chromosome given it a weight $w_i = s_i$.

Now the column mutation. For each locus j we define the count of 0's and 1's as $C_0(j)$ and $C_1(j)$ respectively. These are normalized as

$$n_0(j, t) = \frac{C_0(j)}{C_0(j) + C_1(j)}, \quad n_1(j, t) = \frac{C_1(j)}{C_0(j) + C_1(j)}.$$

These are gathered into the vector $\mathbf{n}(j, t) = (n_0(j, t), n_1(j, t))$ which characterizes the state distribution of j -th locus. In order to direct the current population to a preferred state for locus j we look at the highest weight of row i for locus j taking the value 0 and 1 respectively.

$$\begin{aligned} C'_0(j) &= \max\{W_i | A_{ij} = 0; i = 1, \dots, N\} \\ C'_1(j) &= \max\{W_i | A_{ij} = 1; i = 1, \dots, N\} \end{aligned}$$

which is normalized again

$$n_0(j, t+1) = \frac{C'_0(j)}{C'_0(j) + C'_1(j)}, \quad n_1(j, t+1) = \frac{C'_1(j)}{C'_0(j) + C'_1(j)}.$$

The vector $\mathbf{n}(j, t + 1) = (n_0(j, t + 1), n_1(j, t + 1))$ then provides a direction for the population to evolve against. This characterizes the target state distribution of the locus j among all the chromosomes in the next generation. We have

$$\begin{bmatrix} n_0(j, t + 1) \\ n_1(j, t + 1) \end{bmatrix} = \begin{bmatrix} P_{00}(j, t) & P_{10}(j, t) \\ P_{01}(j, t) & P_{11}(j, t) \end{bmatrix} \begin{bmatrix} n_0(j, t) \\ n_1(j, t) \end{bmatrix}$$

Since the probability must sum to one for the rows in the P-matrix we have

$$P_{00}(j, t) = 1 - P_{01}(j, t), \quad P_{11}(j, t) = 1 - P_{10}(j, t)$$

These conditions allow us to solve for the transition probability $P_{10}(j, t)$ in terms of the single variable $P_{00}j, t$.

$$\begin{aligned} P_{10}(j, t) &= \frac{n_0(j, t + 1) - P_{00}(j, t)n_0(j, t)}{n_1(j, t)} \\ P_{01}(j, t) &= 1 - P_{00}(j, t) \\ P_{11}(j, t) &= 1 - P_{10}(j, t) \end{aligned}$$

We just need to know $P_{00}(j, t)$. We start from $P_{00}(j, t = 0) = 0.5$ and then choose $P_{00}(j, t) = n_0(j, t)$

Summary

2.6 Summary and conclusion

2.7 Outlook / Perspective

- What did we not cover?
- What kind of further investigations does this study invite?

Things to include here

- Could be valuable to spend more time on the validation of the MD simulations. How does material choice and potential effects the results. How realistic is the simulations?
- Are there any interesting approaches for compressed kirigami structures?
- How does these results scale? I imagined that the nanomachine systems should be applied in small units to avoid scaling problems, but in general I could spend way more time on the scaling investigation.
- Since the normal force is applied at the pull blocks the normal force distribution changes from the sides more towards and even distribution as the sheet is put under tension (stretched). If we imagined a sheet for which the center part was either a different material or had some kind of pre-placed asperity on it, could we then exploit this force distribution to get exotic properties as well? By studying this we might get a clearer understanding of what is the cause of my results.
- Possibility to study hysteresis effects. Maybe the frictional behaviours change significantly through repeated cycles of stretch and relax.

Appendices

Appendix A

Appendix B

Bibliography

- [1] F. Bonelli, N. Manini, E. Cadelano and L. Colombo, *Atomistic simulations of the sliding friction of graphene flakes*, .